Supporting Information

Fast Na^+ Kinetics and Suppressed Voltage Hysteresis Enabled by a High-Entropy Strategy for Sodium Oxide Cathodes

Xian-Zuo Wang, Yuting Zuo, Yuanbin Qin, Xu Zhu, Shao-Wen Xu, Yu-Jie Guo, Tianran Yan, Liang Zhang, Zhibin Gao, Lianzheng Yu, Mengting Liu, Ya-Xia Yin, Yonghong Cheng*, Peng-Fei Wang* and Yu-Guo Guo**

Experimental Section

Materials synthesis: In this study, solid-state method was used to synthesis powdery $Na_{0.8+0.1x}Ni_{0.2}Fe_{0.2}Co_{0.2}Mn_{0.2}Ti_{0.2-0.05x}Cu_{0.05x}O_2$ (x = 0, 0', 1, 2', and 2, denoted as NaNFCMTC-0, NaNFCMTC-0', NaNFCMTC-1, NaNFCMTC-2', and NaNFCMTC-2, respectively) and $NaNi_{1/3}Fe_{1/3}Mn_{1/3}O_2$ (NaNFM) with the precursors of Na_2CO_3 (99.8%), NiO (99%), Fe_2O_3 (99%), Co_3O_4 (99.5%), MnO_2 (99%), TiO_2 (99%), and CuO (99%), where Na_2CO_3 and Fe_2O_3 were purchased from Sinopharm Chemical Reagent Co., Ltd., while NiO, Co_3O_4, MnO_2, TiO_2, and CuO were purchased from Aladdin Chemical Reagent Co., Ltd. All these precursors were weighed based on their stoichiometric ratios except Na_2CO_3 which was 5 wt% excess to compensate for its possible loss under calcination. A planetary ball mill was used to mix the precursors thoroughly with an appropriate amount of ethanol as a dispersant for 4h. The mixture was dried at 80 °C for 2 h, pressed into pellets under the pressure of 16 MPa, and then calcined at 950 ℃ for 15 h in a muffle furnace. The obtained cooling samples were fully ground and kept in an argon-filled glove box.

Materials characterization: To confirm the crystalline structures, X-ray diffraction (XRD) was carried out in a Bruker D8 Advance equipped with Cu Kα (λ = 1.5418 Å) X-ray source and the results were refined in TOPAS software using Rietveld method. The structural model of our work is based on the crystallographic information file (CIF) of $NaCrO_2$ (PDF#88-0720, S.G. $R\bar{3}m$ (166)), where Na, Cr, and O locate at *3a, 3b, and 6c* sites, respectively. The Cr site representing the transition metal is replaced with the corresponding occupancy of Ni, Fe, Co, Mn, Ti, and Cu in the designed materials and the occupancy of Na is also modified based on the actual content. For *in-situ* XRD characterization, a special Swagelok cell was used, where an aluminum window was equipped for the penetration of X-ray. The morphologies were detected by a field-emission scanning electron microscope (ZEISS, GEMINI 500). High-

resolution transmission electron microscopy (HRTEM) images were obtained using a Lorenz TEM (Talos F200X). Energy-dispersive spectroscopy (EDS) elemental mapping was conducted on SEM and TEM, respectively, for particles of different sizes. Scanning transmission electron microscopy (STEM) with annular bright-field (ABF) and high angle annular dark-field (HAADF) was performed on a HITACHI HF5000, where the selected area electron diffraction (SAED) was conducted on the same instrument. X-ray photoelectron spectroscopy (XPS) measurements were conducted using a ThermoFisher Scientific ESCALAB Xi+ equipment to determine the valence states of cations in the pristine powder. Inductively coupled plasma mass spectrometry (ICP-MS) was performed using a PerkinElmer NexION 350D ICP-MS apparatus to confirm the real chemical composition. X-ray absorption spectroscopy (XAS) was measured from beamline 13SSW of Shanghai Synchrotron Radiation Facility, and ATHENA software package was utilized to analyze and process the XAS data.

The configurational entropy (S_{config}) is calculated according to the following equation: $S_{config} = -R\left[(\sum_i^n x_i\, lnx_i)_{cation} + \left(\sum_j^m x_j\, lnx_j\right)_{anion}\right]$, where R stands for the gas constant, x_i stands for the concentration of component i in cations, x_j stands for the concentration of component j in anions, n stands for the number of cation species, m stands for the number of anion species. It is worth mentioning that this work focuses on the configurational entropy of the transition metal skeleton, so Na and O are not taken into account. Take $Na_{0.9}Ni_{0.2}Fe_{0.2}Co_{0.2}Mn_{0.2}Ti_{0.15}Cu_{0.05}O_2$ as an example: $S_{config} = -R[0.2\ln(0.2) + 0.2\ln(0.2) + 0.2\ln(0.2) + 0.2\ln(0.2) + 0.15\ln(0.15) + 0.05\ln(0.05)] \approx 1.72R$.

Electrochemical testing: To obtain the working cathodes, 75 wt% active cathode materials, 15 wt% conductive additives (Super P) and 10 wt% polyvinylidene fluoride (PVDF) with appropriate amount of N-methyl-2-pyrrolidone (NMP) were mixed into a slurry, spread on the carbon-coated Al foil, and then dried at 80 ℃ for 12 h using a vacuum oven. The loading mass of the active material on cathode was about 2−3 mg cm^{-2}. Hard carbon (HC), Super P, and PVDF in a weight ratio of 7.5:1.5:1.0 were mixed in NMP and fabricated into electrodes in the same way for the anode in the full cell, while sodium metal was used as the anode in the half cell. The sodium foil used as anode in the half cell is prepared from sodium ingot (99.8%, Alfa Aesar), where the oxide layer on the surface is removed with a ceramic knife. The metal sodium is hammered and rolled into 0.3−0.5 mm thick foil and then punched into 12 mm diameter circular electrodes. Glass fibers (GF/D, Whatman) were utilized as the separator, and 1 M $NaClO_4$ was dissolved in propylene carbonate (PC) containing 5 vol% fluoroethylene carbonate (FEC) for the electrolyte. All of the above materials were assembled into CR2032 coin cells in

a glove box filled with argon (H_2O, $O_2 \leq 0.1$ ppm) for the subsequent electrochemical performance tests. Galvanostatic charge/discharge (GCD) measurements were carried out within the voltage range of 2.2−4.1 V (vs. Na^+/Na) by a Land 2001A test system at room temperature (25℃). The full cells were tested within the voltage range of 1.5−4.1 V and the ratio of capacity for anode to cathode is controlled within the range of 1.05−1.10. It should be mentioned that the HC anode was electrochemically presodiated before assembly to gain a stable solid electrolyte interphase (SEI) and reduce the impact of the low Coulombic efficiency of HC. The cyclic voltammetry (CV) measurements were conducted at different scan rates of 0.1, 0.2, 0.4, 0.6, 0.8, and 1.0 mV s^{-1} on an Autolab-M204 electrochemical workstation. Electrochemical impedance spectroscopy (EIS) was collected using the same Autolab workstation by imposing a 5 mV AC signal in the frequency range of 10^{-3}–10^5 Hz on the half cell which has been cycled five times to get a stable cathode electrolyte interphase (CEI), and the results were fitted utilizing ZView software. Galvanostatic intermittent titration technique (GITT) was measured by applying the repeated current pulses at a current density of 22 mA g^{-1} (0.1 C) for 30 min followed by relaxation of 10 h.

The Na^+ diffusion coefficient (D_{Na^+}) calculation by GITT results is according to the following equation: $D_{Na^+} = \frac{4}{\pi\tau}(\frac{m_b V_m}{M_b S})^2(\frac{\Delta E_s}{\Delta E_\tau})^2$, where τ stands for the constant current pulse time (s), m_b stands for the weight of active materials (g), M_b stands for the molecular weight of the cathode materials (g mol^{-1}), V_m represents the molar volume of cathode (cm^3 mol^{-1}), S represents the area of electrode (cm^2), ΔE_s stands for the steady-state voltage variation before and after the pulse, ΔE_τ stands for the voltage difference during the constant current pulse.

The Na^+ diffusion coefficient (D_{Na^+}) calculation by CV results at different scan rates is according to the Randles-Sevcik equation: $I_P = 0.4463n^{3/2}F^{3/2}CSR^{-1/2}T^{-1/2}D_{Na^+}^{1/2}v^{1/2}$, where I_P represents the peak current (A), n represents the number of moles of electrons transferred in the reaction, F represents the Faraday constant (96485 C mol^{-1}), C represents the Na^+ concentration in the lattice (mol cm^{-3}), S represents the area of electrode (cm^2), R represents the gas constant (8.314 J mol^{-1} K^{-1}), T represents the absolute temperature (calculated at room temperature 298 K), v represents the scan rate (V s^{-1}).

DFT Calculations: All computations pertaining to NaNFCMTC-1 and NaNFM were executed employing the Vienna Ab-initio Simulation Package (VASP 5.4.4).[S1] The Perdew-Burke-Ernzerh of (PBE)[S2] parameterization in conjunction with the projector-augmented wave (PAW) method was adopted. GGA+U[S3] was integrated into this study, with the U values for Ni, Fe, Co, Mn, Ti, and Cu set at 6.1, 4.5, 5.2, 4.0, 3.4, and 6.0 eV, respectively.[S4] The kinetic

energy cutoff value for plane wave expansion in reciprocal space was established at 500 eV. Given that the lattice parameters of the supercell models examined in this study exceeded 10 Å in the a, b, and c crystallographic directions, we employed a Monkhorst-Pack 1×1×1 k-grid for numerical integrations within the first irreducible Brillouin zone. During structural optimizations, the convergence criteria for atomic forces and total energy were set at 0.05 eV/Å and 10^{-5} eV, respectively. Additionally, a force convergence criterion of 0.05 eV $Å^{-1}$ was employed for relaxation. With a time step of 1 fs, the Nose thermostat was used to simulate an overall duration of 10 ps for first-principles molecular dynamics calculations in the temperature range of 600−900 K. Ionic diffusion behavior was assessed via time-dependent mean square displacement (MSD) and diffusion coefficient (D): $MSD(t) = \langle |r(t) - r(0)|^2 \rangle$, $D = \frac{1}{6} \lim_{t \to \infty} \frac{\mathrm{d}}{\mathrm{d}t} \langle r^2(t) \rangle$, where $r(t)$ is the position of the ion at the time t. Subsequently, according to the Arrhenius equation, the diffusion coefficients at varying temperatures were used for computing to obtain the migration energy barrier.

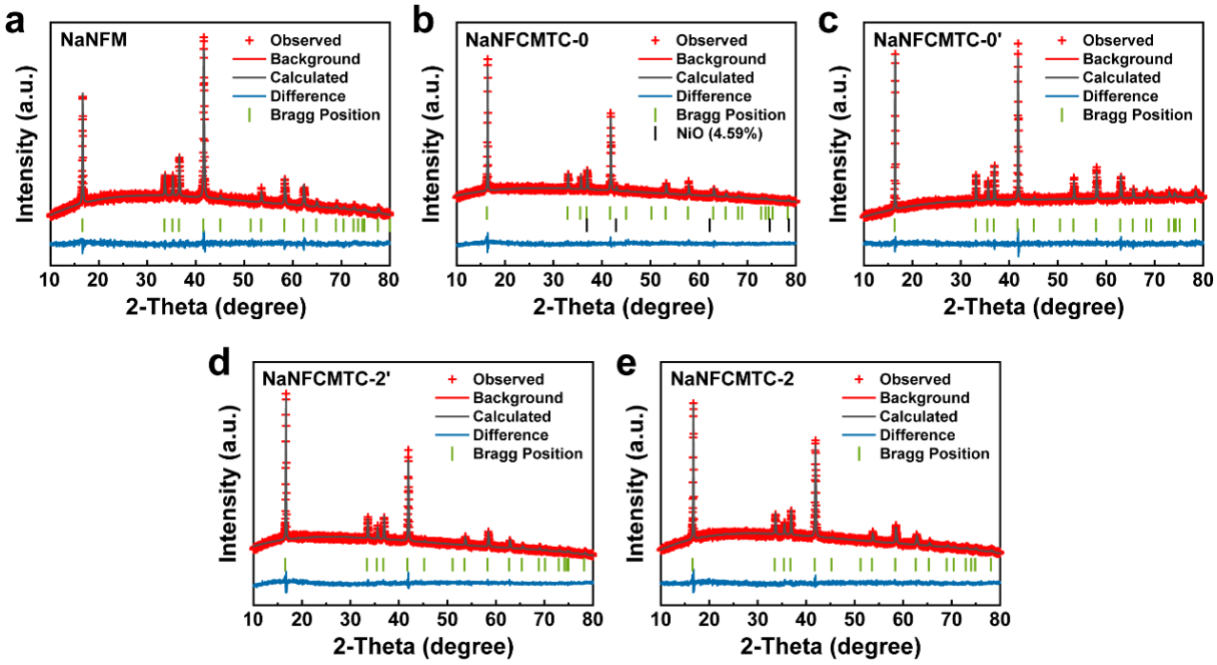

Figure S1. Rietveld refinement patterns of the powder XRD data for a) NaNFM, b) NaNFCMTC-0, c) NaNFCMTC-0', d) NaNFCMTC-2', and e) NaNFCMTC-2.

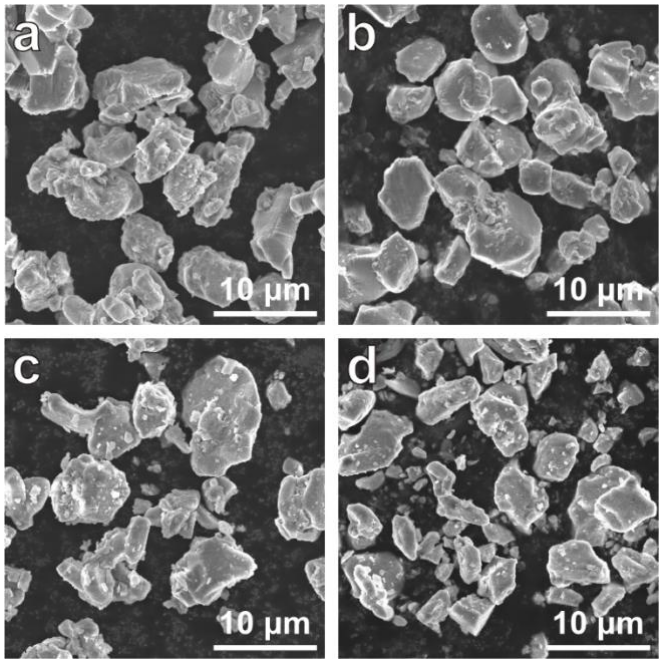

Figure S2. SEM images of a) NaNFCMTC-0, b) NaNFCMTC-0', c) NaNFCMTC-2', and d) NaNFCMTC-2.

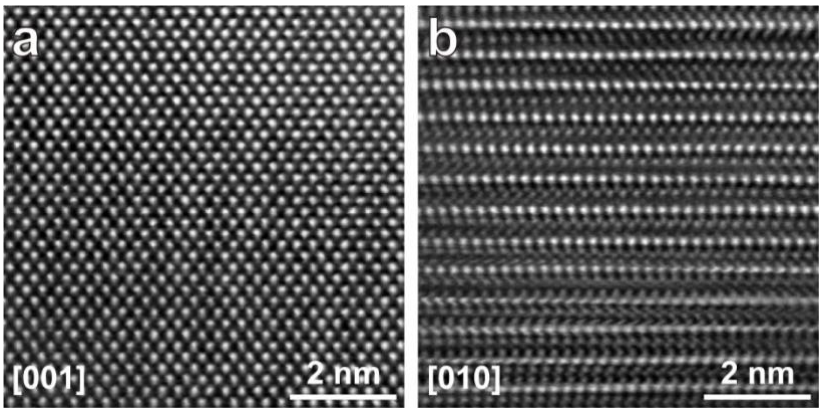

Figure S3. Bright field images of NaNFCMTC-1 from the zone axis of a) [001] and b) [010] directions.

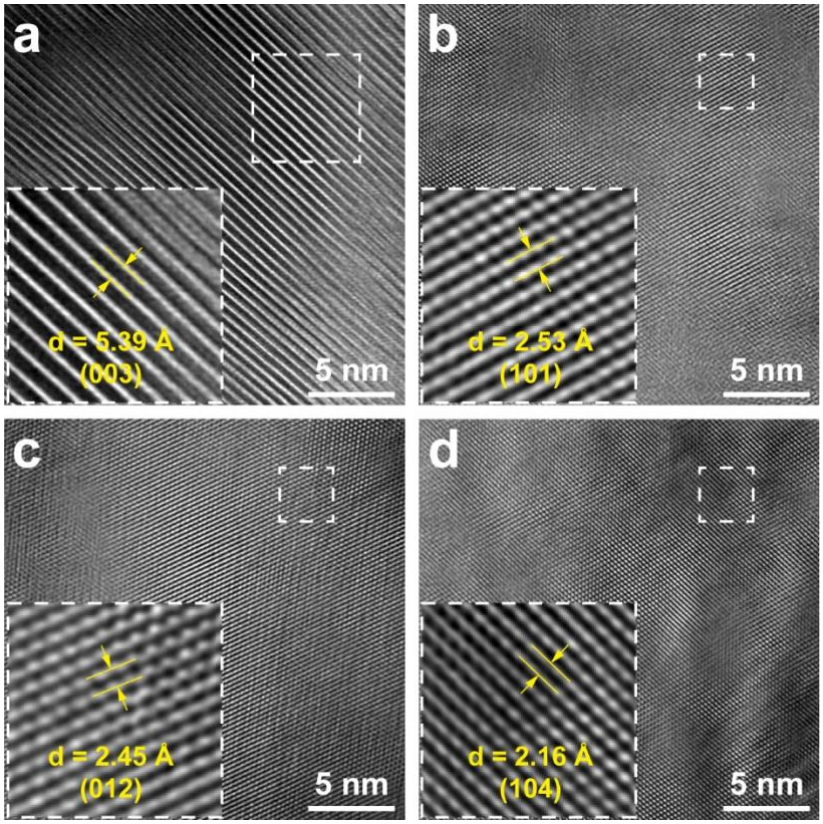

Figure S4. HRTEM images of NaNFCMTC-1 for a) lattice plane (003), b) lattice plane (101), c) lattice plane (012), and d) lattice plane (104).

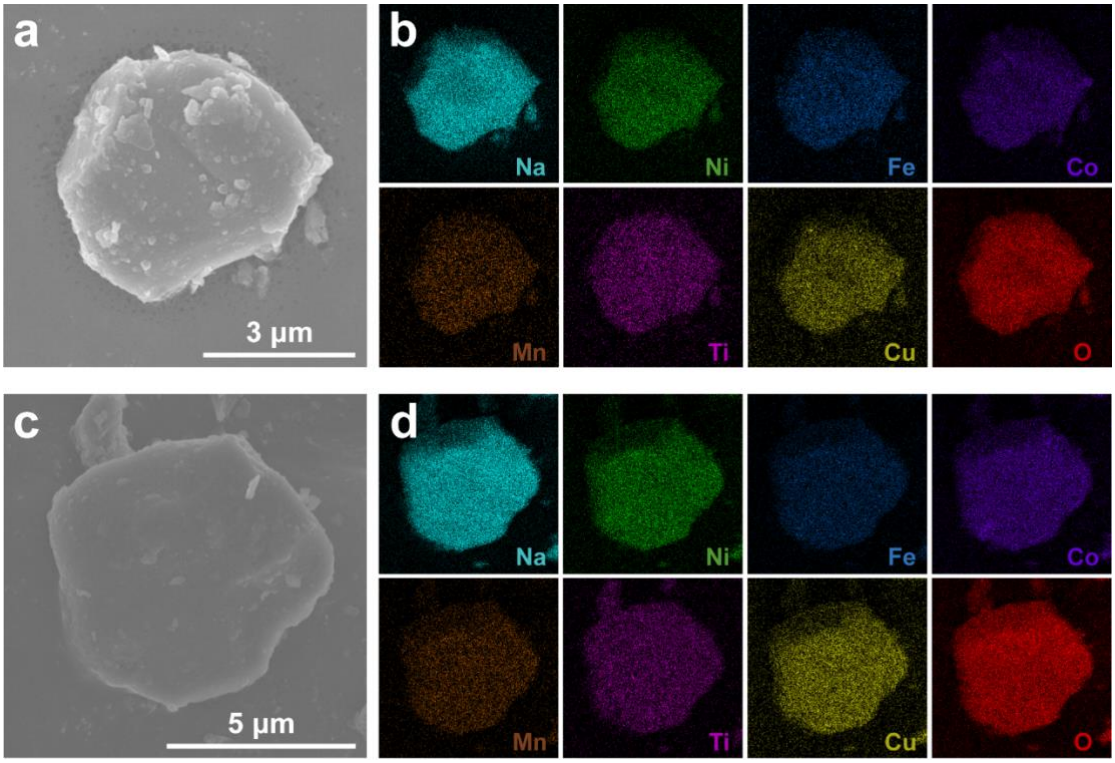

Figure S5. a) SEM image and b) EDS elemental mappings of larger NaNFCMTC-1 particle (No.1). c) SEM image and d) EDS elemental mappings of larger NaNFCMTC-1 particle (No.2).

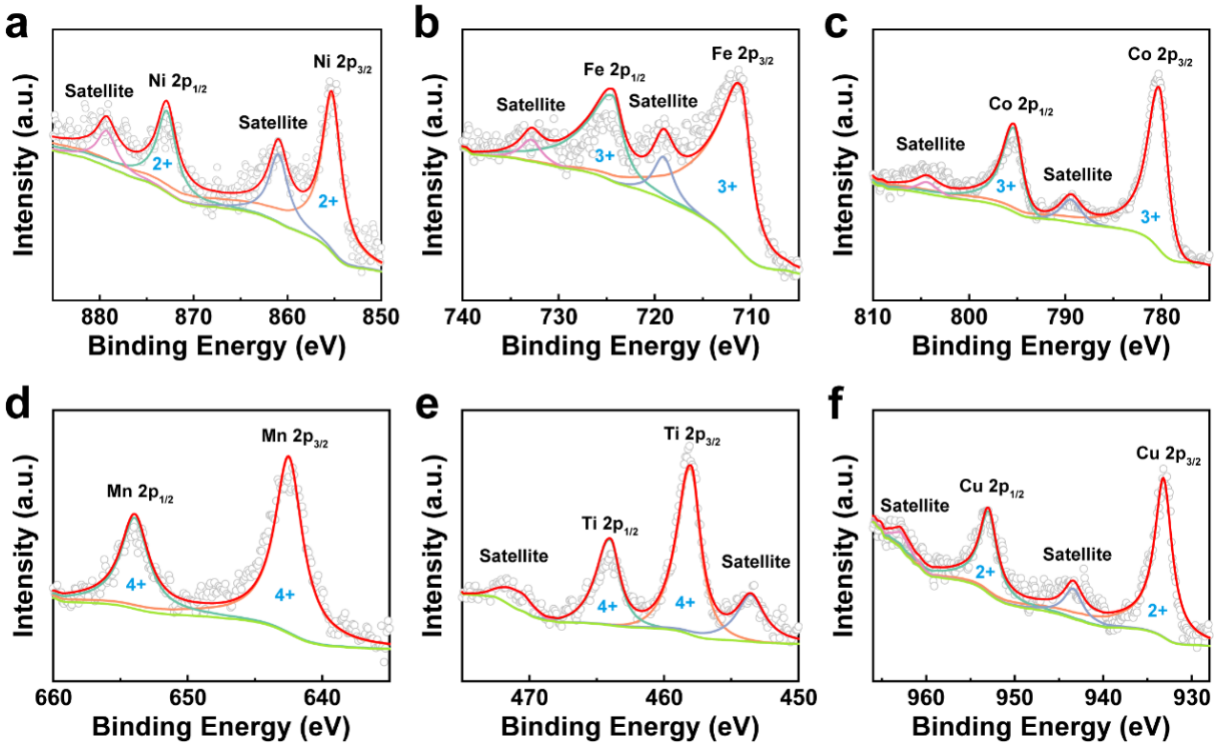

Figure S6. XPS spectra of the NaNFCMTC-1 powder in (a) Ni 2p, (b) Fe 2p, (c) Co 2p, (d) Mn 2p, e) Ti 2p, and (f) Cu 2p. Corresponding valence states are Ni^{2+} ($2p_{1/2}$ binding energy of 872.87 eV and $2p_{3/2}$ of 855.28 eV), Fe^{3+} ($2p_{1/2}$ binding energy of 724.37 eV and $2p_{3/2}$ of 711.01 eV), Co^{3+} ($2p_{1/2}$ binding energy of 795.36 eV and $2p_{3/2}$ of 780.22 eV), Mn^{4+} ($2p_{1/2}$ binding energy of 653.95 eV and $2p_{3/2}$ of 642.49 eV), Ti^{4+} ($2p_{1/2}$ binding energy of 463.99 eV and $2p_{3/2}$ of 457.99 eV), and Cu^{2+} ($2p_{1/2}$ binding energy of 952.98 eV and $2p_{3/2}$ of 933.19 eV).

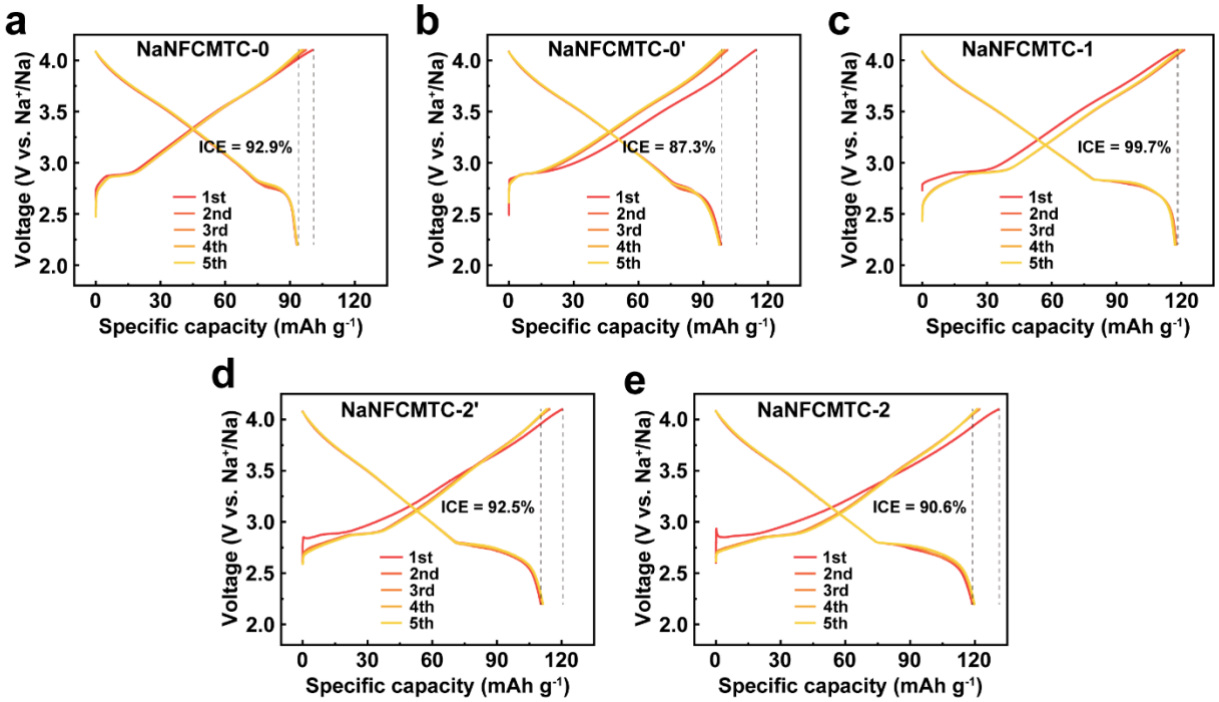

Figure S7. GCD curves of a) NaNFCMTC-0, b) NaNFCMTC-0', c) NaNFCMTC-1, d) NaNFCMTC-2', and e) NaNFCMTC-2 at 0.1 C.

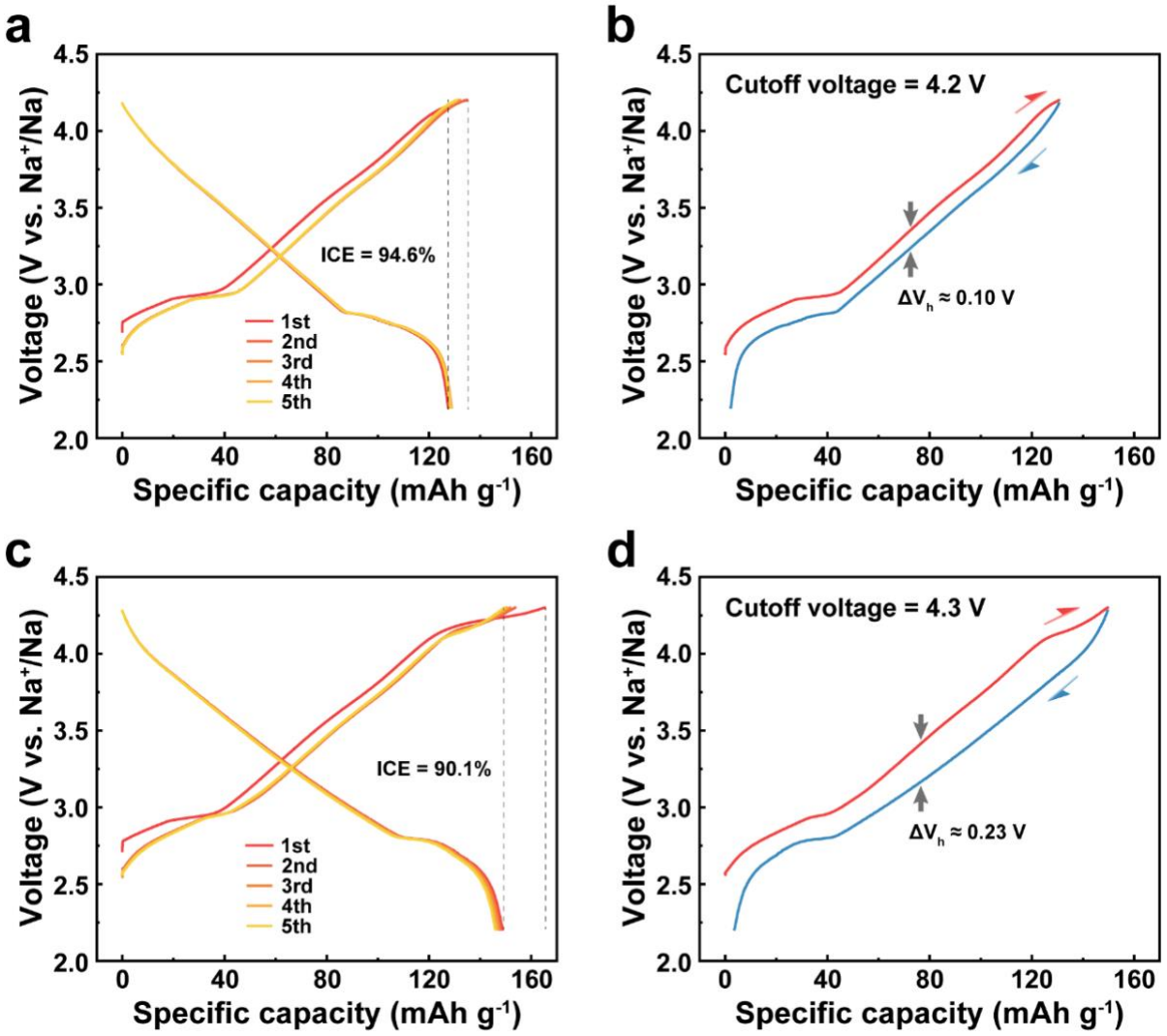

Figure S8. Performance after increasing the cutoff voltage of NaNFCMTC-1. a) GCD curves at 0.1 C and b) corresponding voltage hysteresis within the voltage range of 2.2−4.2 V. c) GCD curves at 0.1 C and d) corresponding voltage hysteresis within the voltage range of 2.2−4.3 V.

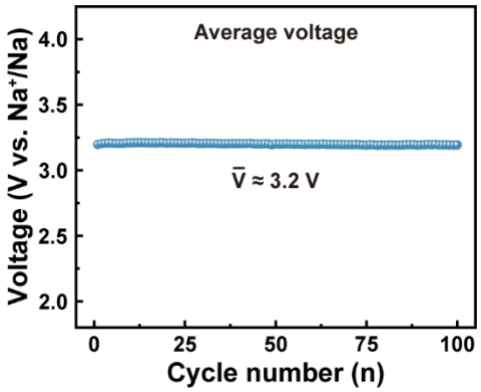

Figure S9. Average voltage of NaNFCMTC-1 over 100 cycles at 0.1C.

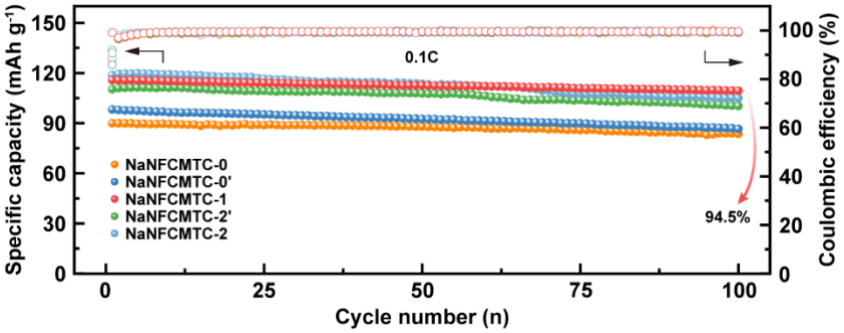

Figure S10. Cycling performance of five cathodes at 0.1 C rate.

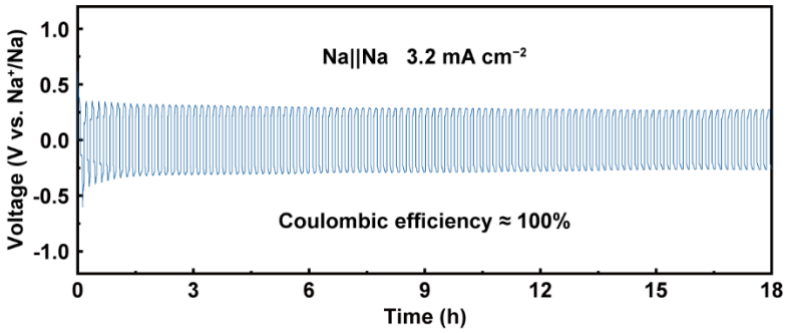

Figure S11. Long cycle performance of Na||Na symmetric batteries at a current density of 3.2 mA cm^{-2}.

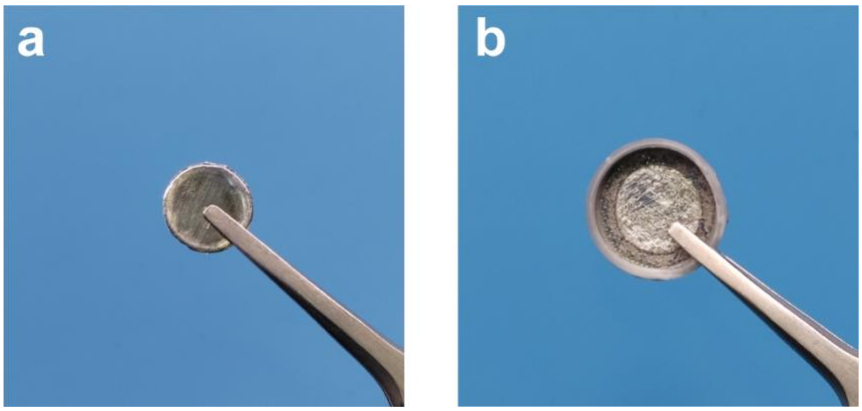

Figure S12. The optical photograph of a) fresh Na foil and b) Na foil after 2000 cycles (the glass fibers adhered on the surface have been scraped off).

The mass of our used sodium foil (calculated according to 0.3 mm thick) is:

$$m_{Na} = \rho \times V = 0.968 \times \pi \times 0.6^2 \times 0.03 \approx 0.03284\ g$$

The theretical specific capacity of Na anode is:

$$C = 26.8 \times \frac{n}{M} = 26.8 \times \frac{1}{23} \approx 1165.2\ mAh\ g^{-1}$$

Therefore the capacity of Na anode is calculated to be:

$$C_{Na} = C \times m_{Na} = 0.03284 \times 1165.2 \approx 38.27\ mA\ h$$

In comparison, the capacity of cathode side (even based on 10 mg cm^{-2} mass loading) is calculated to be:

$$C_{NaNFCMTC-1} = C_1 \times m_1 = 117 \times 10 \times 0.785 \times 10^{-3} \approx 0.91845\ mA\ h$$

The capacity of Na metal far exceeds the cacapicty of NaNFCMTC-1 cathode and the average Coulombic efficiency of Na||Na cell is nearly 100% at 5C, which make the prepared sodium foil maintain for thousands of cycles.

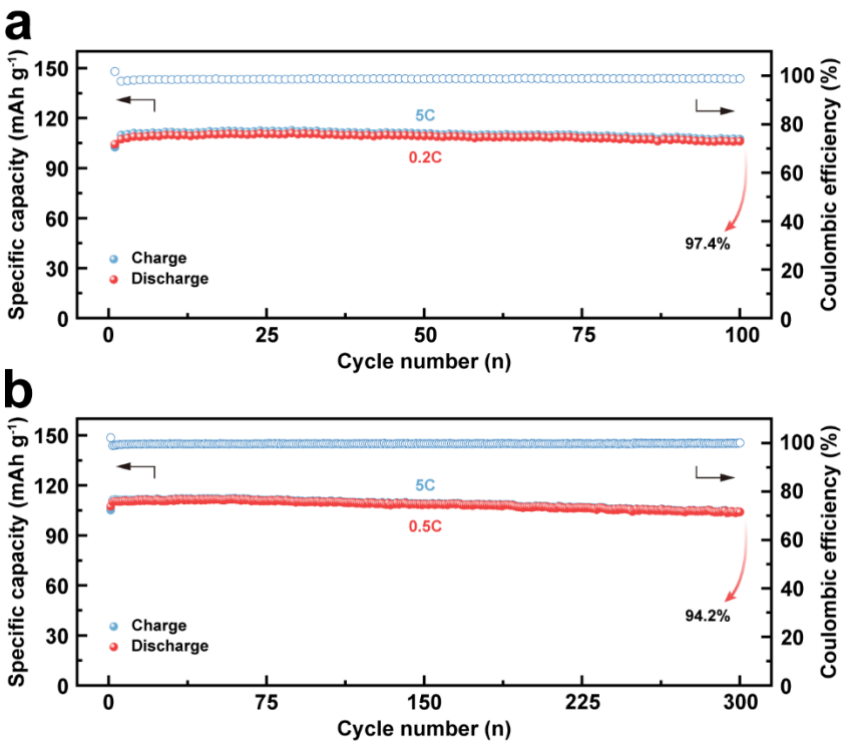

Figure S13. Fast-charge slow-discharge performance of NaNFCMTC-1. a) Charge at 5 C and discharge at 0.2 C. b) Charge at 5 C and discharge at 0.5 C.

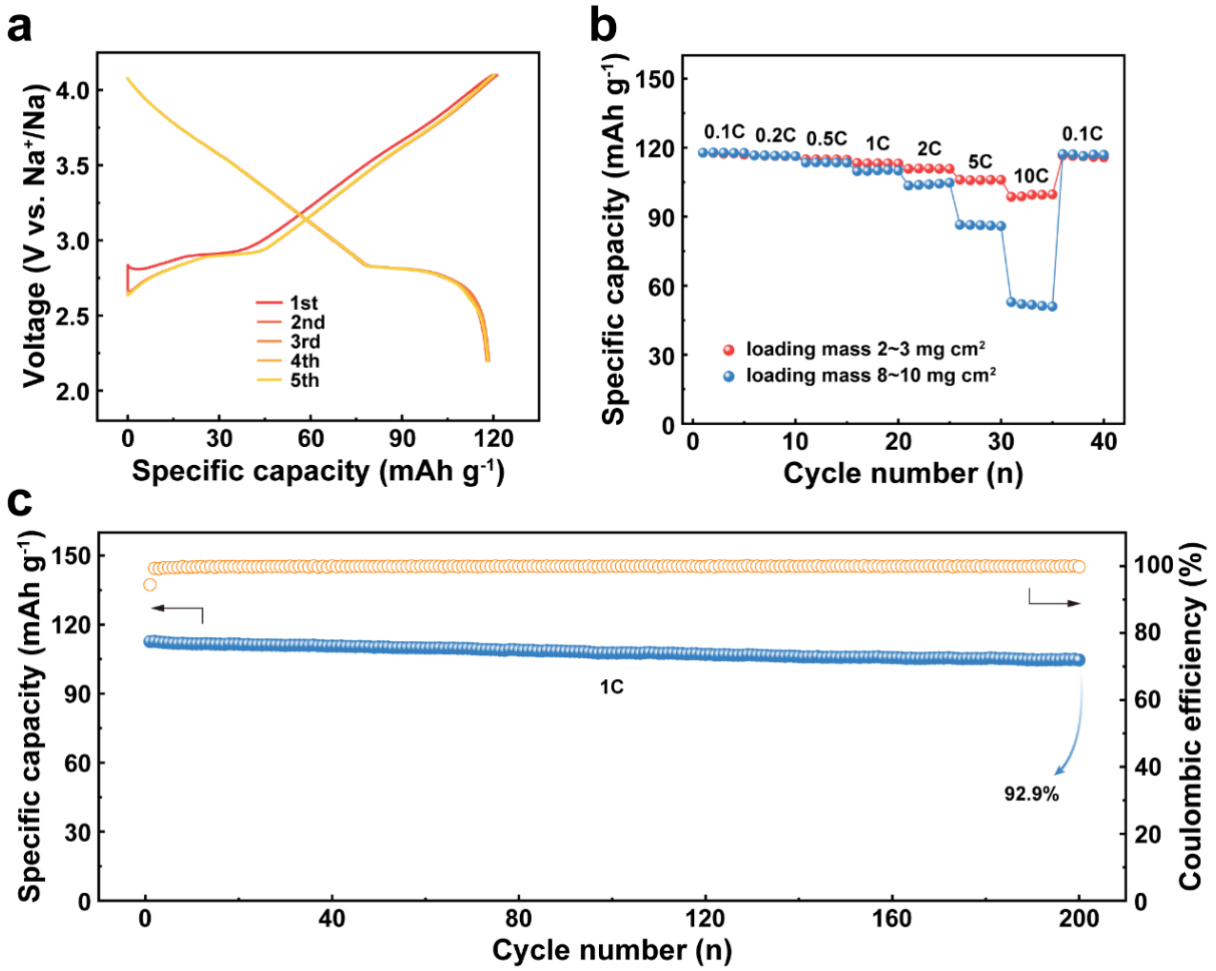

Figure S14. Electrochemical performance of NaNFCMTC-1 cathode with higher mass loading of 8−10 mg cm^{-2}. a) GCD curves at 0.1 C. b) Rate performance comparison between different mass loading cathodes. c) Cycling performance at 1 C rate.

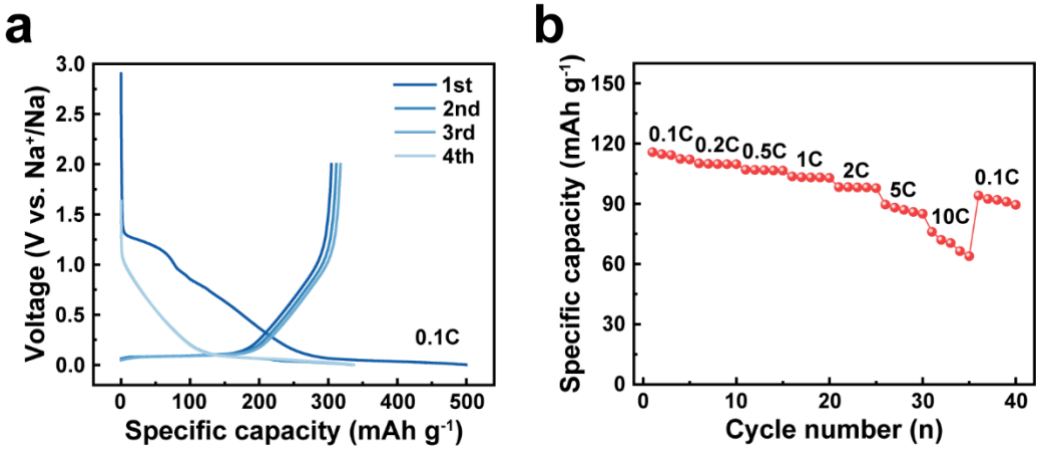

Figure S15. a) Initial GCD curves of HC anode at a current of 30 mA g^{-1} within the voltage range of 0.001−2.0 V. b) Rate performance of NaNFCMTC-1||HC full-cell within the voltage range of 1.5−4.1 V.

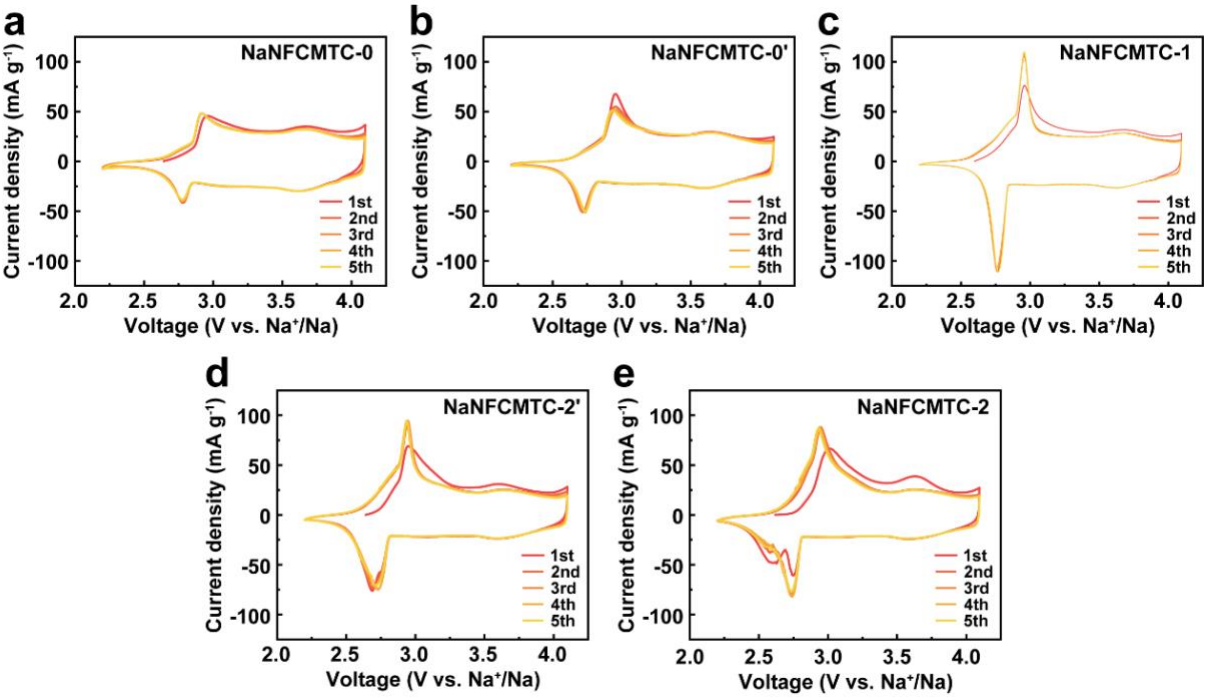

Figure S16. CV curves of a) NaNFCMTC-0, b) NaNFCMTC-0', c) NaNFCMTC-1, d) NaNFCMTC-2', and e) NaNFCMTC-2 at a scan rate of 0.1 mV s^{-1} within the voltage range of 2.2−4.1 V.

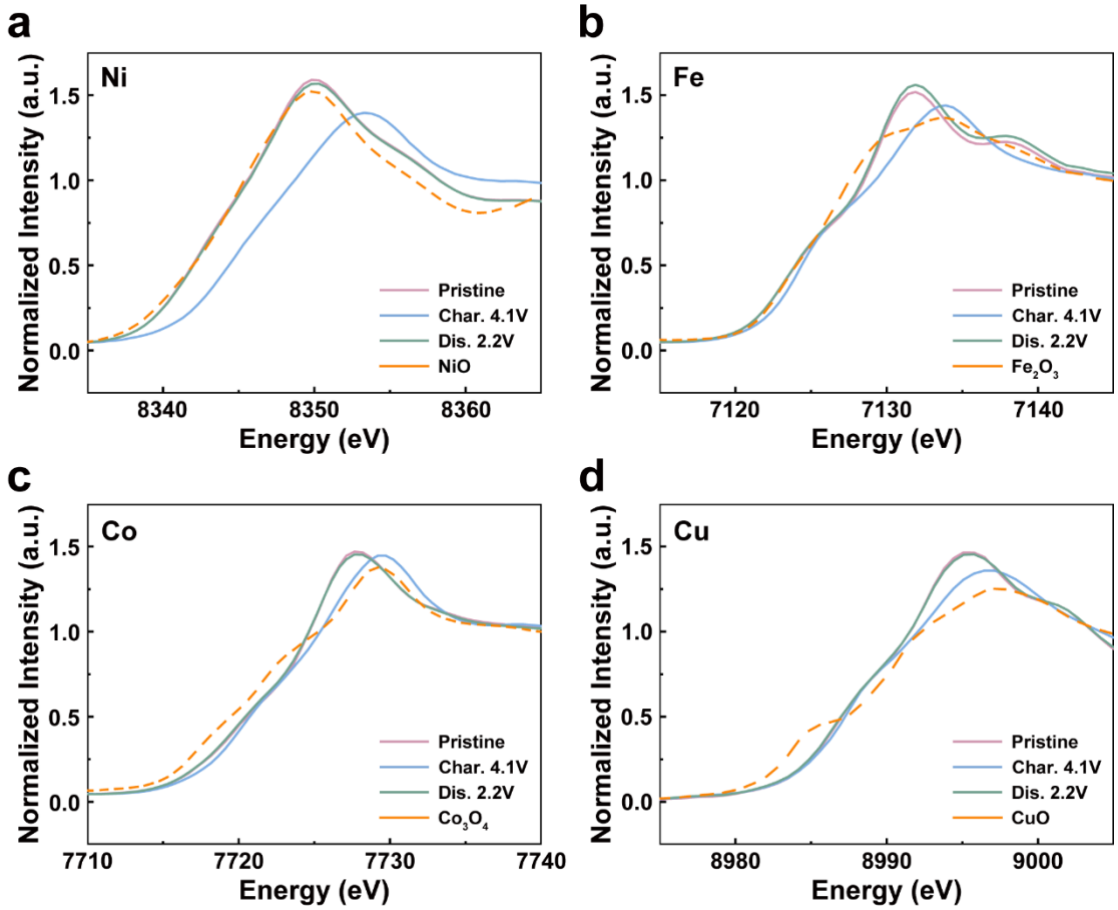

Figure S17. Normalized ex-situ XANES spectra for a) Ni K-edge, b) Fe K-edge, c) Co K-edge, and d) Cu K-edge of NaNFCMTC-1 cathode with reference compounds.

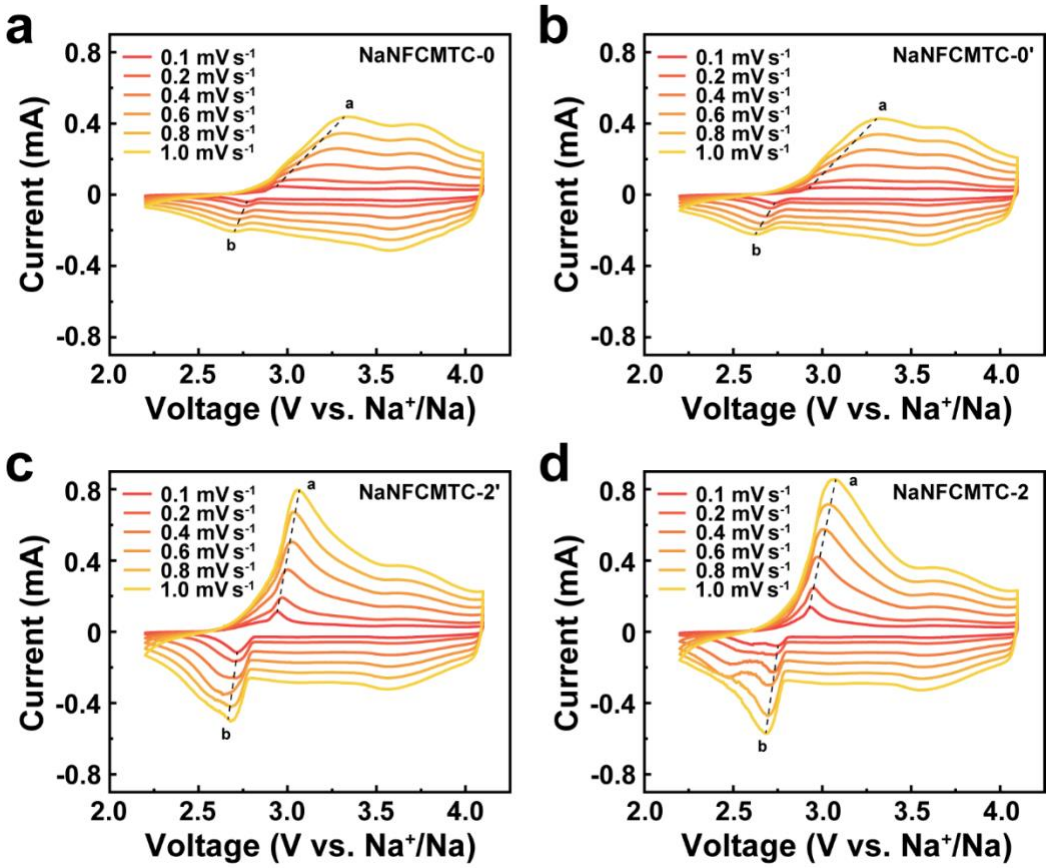

Figure S18. CV curves within the voltage range of 2.2−4.1 V at different scan rates from 0.1 to 1.0 mV s^{-1} of a) NaNFCMTC-0, b) NaNFCMTC-0', c) NaNFCMTC-2', and d) NaNFCMTC-2.

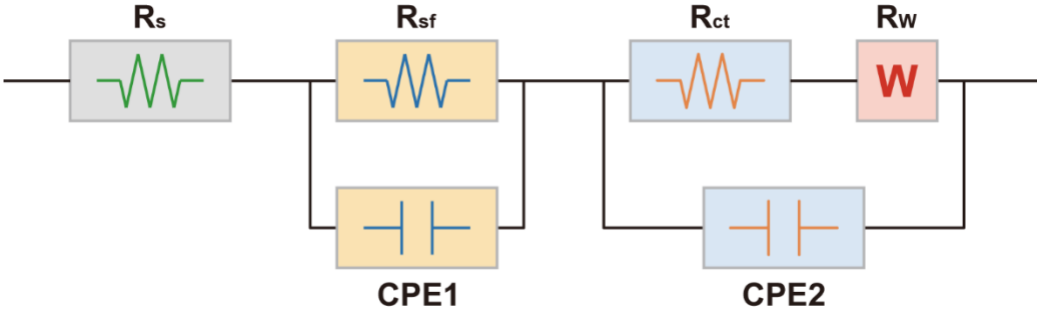

Figure S19. Equivalent circuit for EIS fitting. R_s is considered as the Ohmic resistance, including bulk resistance or other resistance from the separator and electrolyte. R_{sf} in the high-frequency region represents the interfacial impedance of Na^+ across the CEI, and R_{ct} in the midfrequency region interprets the implication of charge transfer impedance. Lastly, R_w in the

low-frequency tail is the Warburg impedance dominated by the mass transfer processes, which represents the diffusion performance of Na^+ in the material.

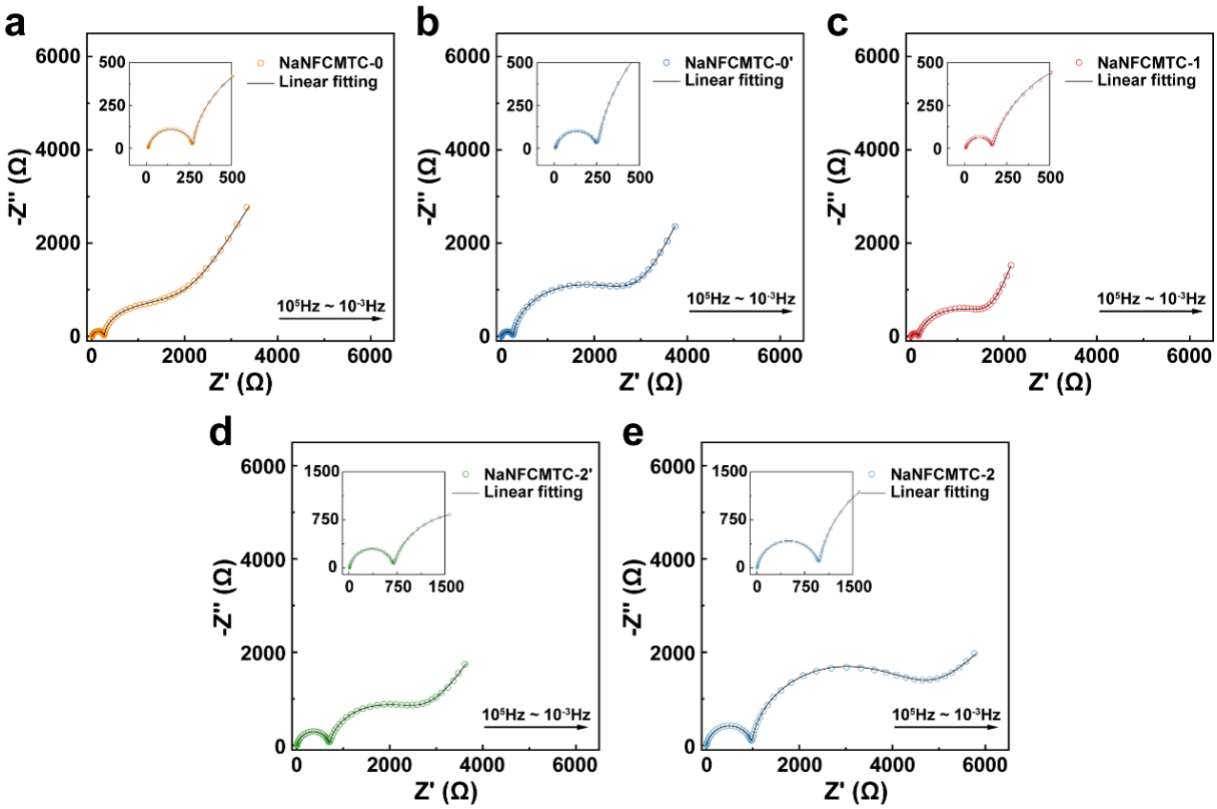

Figure S20. Nyquist plots and the fitting curves at the fully discharged state after five cycles of a) NaNFCMTC-0, b) NaNFCMTC-0', c) NaNFCMTC-1, d) NaNFCMTC-2', and e) NaNFCMTC-2.

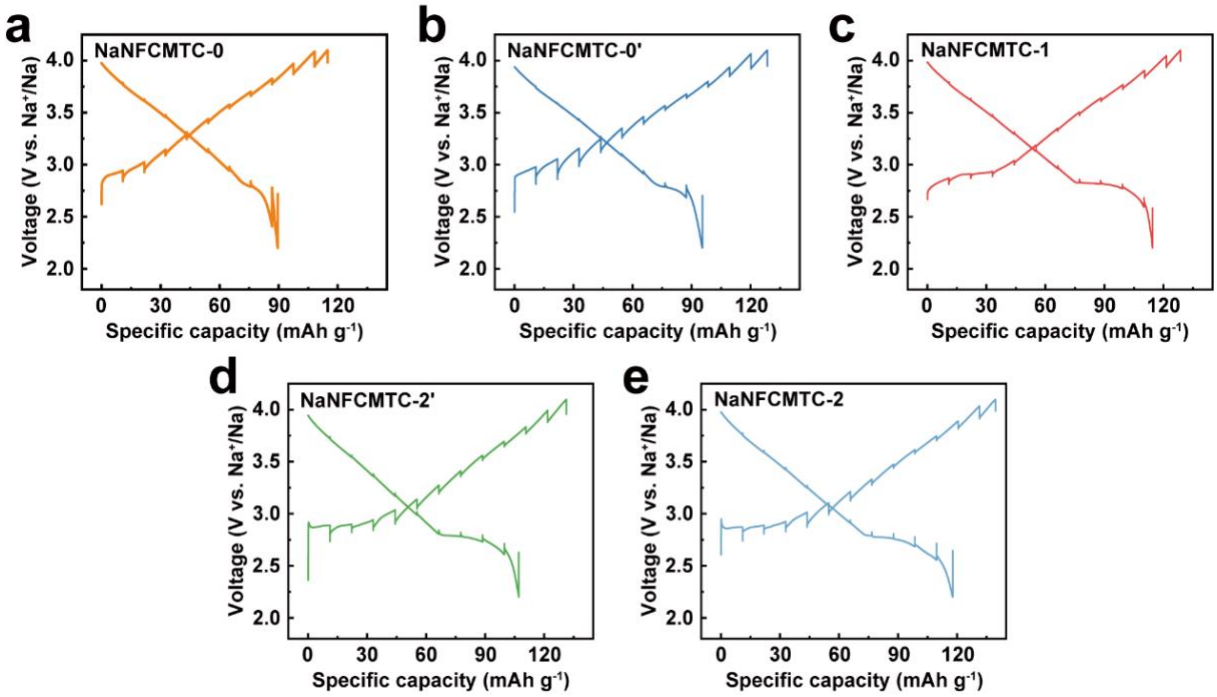

Figure S21. GITT curves of a) NaNFCMTC-0, b) NaNFCMTC-0', c) NaNFCMTC-1, d) NaNFCMTC-2', and e) NaNFCMTC-2 in the first cycle.

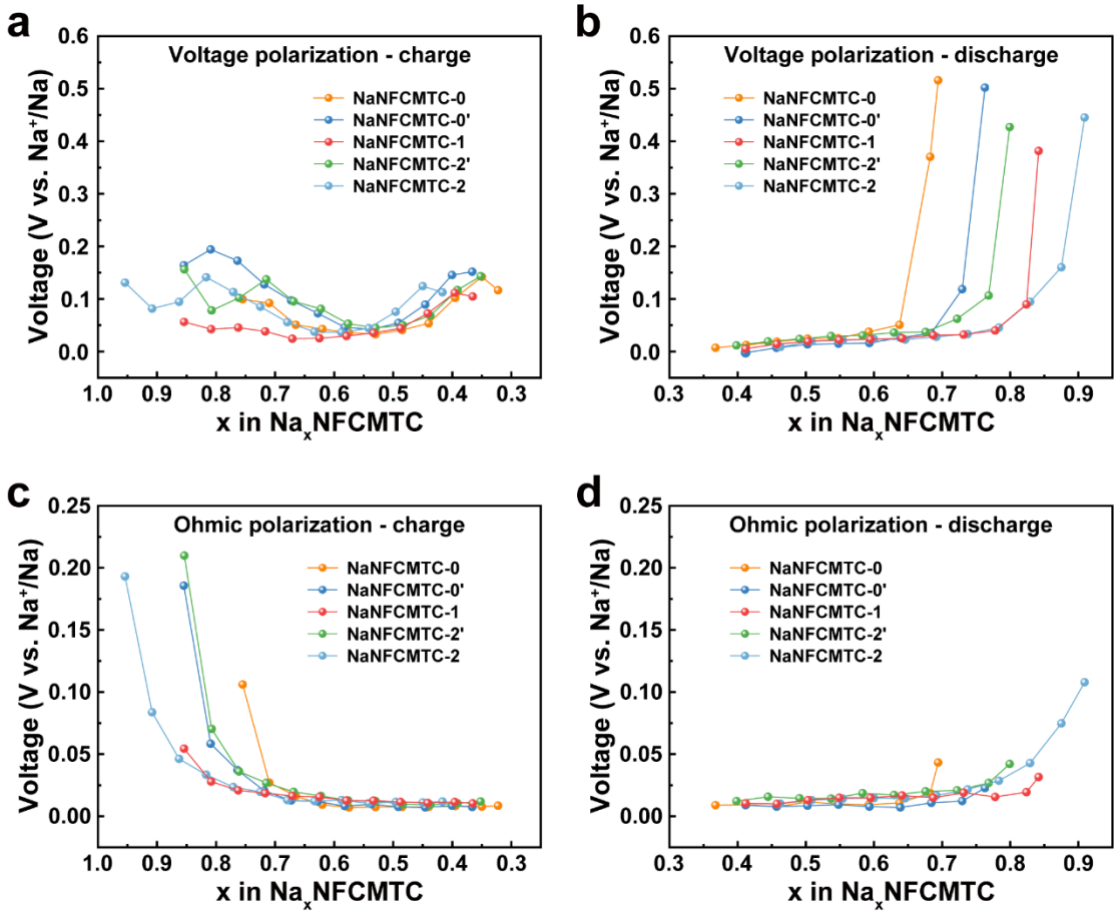

Figure S22. Corresponding voltage polarization in a) charge process and b) discharge process, Ohmic polarization in c) charge process and d) discharge process calculated from the GITT data.

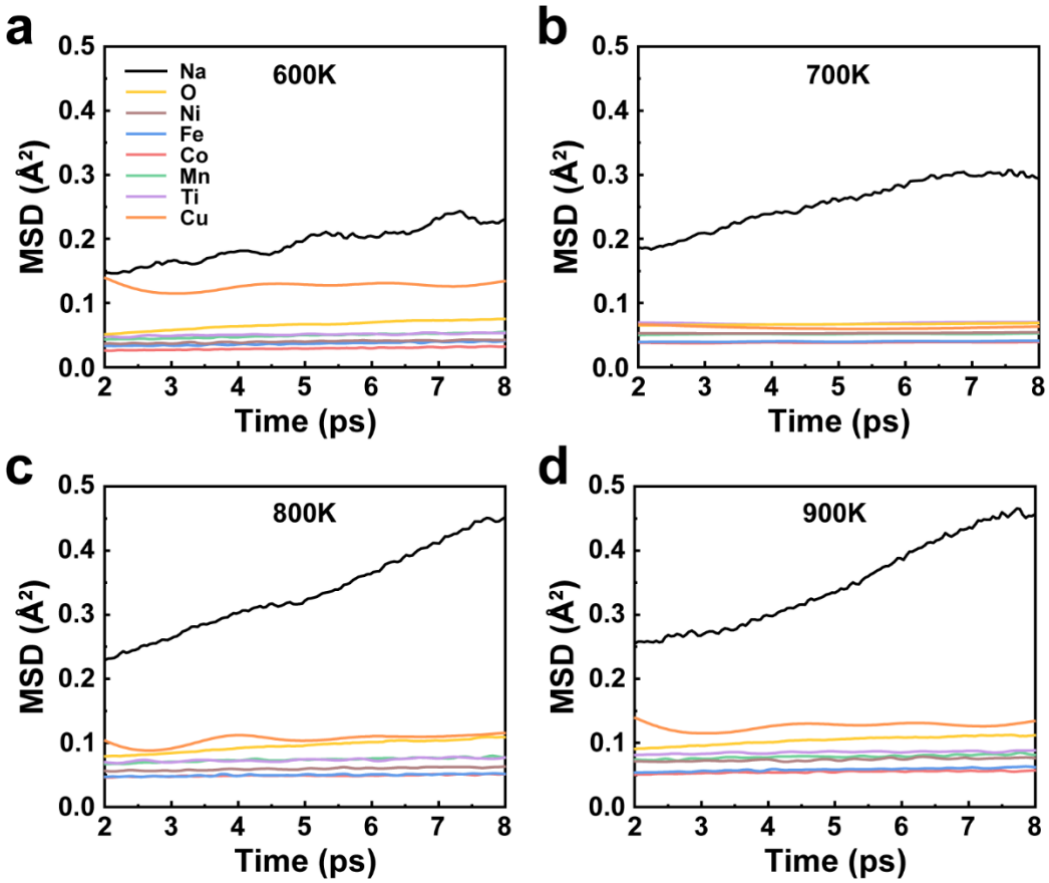

Figure S23. MSD curves for NaNFCMTC-1 at O3 phase simulated in temperatures of a) 600 K, b) 700 K, c) 800 K, and d) 900 K from 2 to 8 ps.

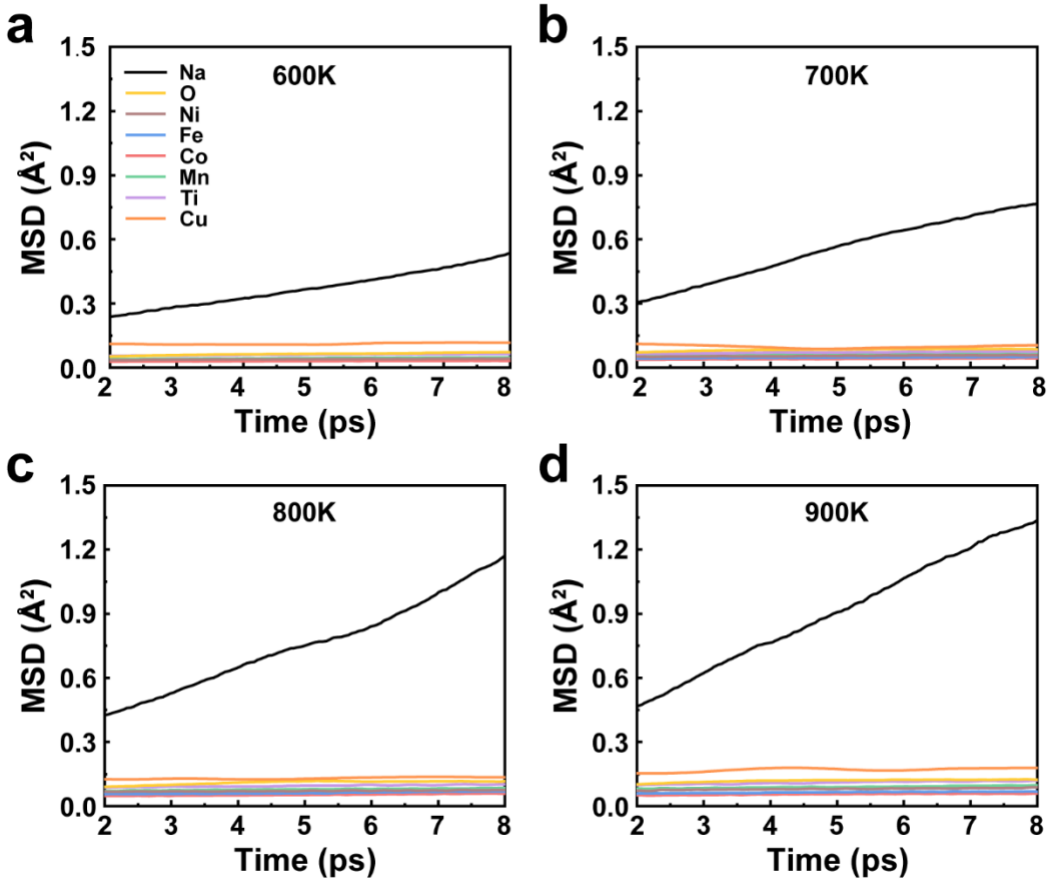

Figure S24. MSD curves for NaNFCMTC-1 at P3 phase simulated in temperatures of a) 600 K, b) 700 K, c) 800 K, and d) 900 K from 2 to 8 ps.

Table S1. Crystallographic parameters of NaNFM refined by Rietveld method.

Atom	Np	x	y	z	Occ.
Na	3a	0	0	0	1.0
Ni	3b	0	0	0.5	1/3
Fe	3b	0	0	0.5	1/3
Mn	3b	0	0	0.5	1/3
O	6c	0	0	0.23612	1.0

a = 2.9830713 Å c = 16.0171583 Å V = 123.43644 Å^3

R_p = 3.03% R_{wp} = 3.83%

Table S2. Crystallographic parameters of NaNFCMTC-0 refined by Rietveld method.

Atom	Np	x	y	z	Occ.

Na	3a	0	0	0	0.8
Ni	3b	0	0	0.5	0.2
Fe	3b	0	0	0.5	0.2
Co	3b	0	0	0.5	0.2
Mn	3b	0	0	0.5	0.2
Ti	3b	0	0	0.5	0.2
O	6c	0	0	0.22804	1.0
a = 2.9512886 Å c = 16.3359984 Å V = 123.22524 Å^3					
R_p = 3.83% R_{wp} = 4.86%					

Table S3. Crystallographic parameters of NaNFCMTC-0' refined by Rietveld method.

Atom	**Site**	**x**	**y**	**z**	**Occ.**
Na	3a	0	0	0	0.9
Ni	3b	0	0	0.5	0.2
Fe	3b	0	0	0.5	0.2
Co	3b	0	0	0.5	0.2
Mn	3b	0	0	0.5	0.2
Ti	3b	0	0	0.5	0.2
O	6c	0	0	0.23025	1.0
a = 2.9534368 Å c = 16.2644505 Å V = 122.86421 Å^3					
R_p = 2.78% R_{wp} = 3.55%					

Table S4. Crystallographic parameters of NaNFCMTC-1 refined by Rietveld method.

Atom	**Np**	**x**	**y**	**z**	**Occ.**
Na	3a	0	0	0	0.9
Ni	3b	0	0	0.5	0.2
Fe	3b	0	0	0.5	0.2
Co	3b	0	0	0.5	0.2
Mn	3b	0	0	0.5	0.2
Ti	3b	0	0	0.5	0.15
Cu	3b	0	0	0.5	0.05

O	6c	0	0	0.23418	1.0

a = 2.9583435 Å c = 16.1912556 Å V = 122.71803 Å^3

R_p = 3.46% R_{wp} = 4.35%

Table S5. Crystallographic parameters of NaNFCMTC-2' refined by Rietveld method.

Atom	**Np**	**x**	**y**	**z**	**Occ.**
Na	3a	0	0	0	0.9
Ni	3b	0	0	0.5	0.2
Fe	3b	0	0	0.5	0.2
Co	3b	0	0	0.5	0.2
Mn	3b	0	0	0.5	0.2
Ti	3b	0	0	0.5	0.1
Cu	3b	0	0	0.5	0.1
O	6c	0	0	0.23141	1.0

a = 2.9606466 Å c = 16.0831485 Å V = 122.08853 Å^3

R_p = 3.71% R_{wp} =4.74%

Table S6. Crystallographic parameters of NaNFCMTC-2 refined by Rietveld method.

Atom	**Np**	**x**	**y**	**z**	**Occ.**
Na	3a	0	0	0	1.0
Ni	3b	0	0	0.5	0.2
Fe	3b	0	0	0.5	0.2
Co	3b	0	0	0.5	0.2
Mn	3b	0	0	0.5	0.2
Ti	3b	0	0	0.5	0.1
Cu	3b	0	0	0.5	0.1
O	6c	0	0	0.23154	1.0

a = 2.9643559 Å c = 16.0376577Å V = 122.04845 Å^3

R_p = 3.23% R_{wp} = 4.11%

Table S7. Stoichiometry of NaNFCMTC-0 compounds determined by ICP-MS.

Theoretical chemical formula	Measured atomic ratio					
	Na	Ni	Fe	Co	Mn	Ti
$Na_{0.8}Ni_{0.2}Fe_{0.2}Co_{0.2}Mn_{0.2}Ti_{0.2}O_2$	0.798	0.199	0.198	0.199	0.197	0.198

Table S8. Stoichiometry of NaNFCMTC-0' compounds determined by ICP-MS.

Theoretical chemical formula	Measured atomic ratio					
	Na	Ni	Fe	Co	Mn	Ti
$Na_{0.9}Ni_{0.2}Fe_{0.2}Co_{0.2}Mn_{0.2}Ti_{0.2}O_2$	0.897	0.201	0.199	0.199	0.198	0.196

Table S9. Stoichiometry of NaNFCMTC-1 compounds determined by ICP-MS.

Theoretical chemical formula	Measured atomic ratio						
	Na	Ni	Fe	Co	Mn	Ti	Cu
$Na_{0.9}Ni_{0.2}Fe_{0.2}Co_{0.2}Mn_{0.2}Ti_{0.15}Cu_{0.05}O_2$	0.898	0.201	0.200	0.199	0.198	0.148	0.050

Table S10. Stoichiometry of NaNFCMTC-2' compounds determined by ICP-MS.

Theoretical chemical formula	Measured atomic ratio						
	Na	Ni	Fe	Co	Mn	Ti	Cu
$Na_{0.9}Ni_{0.2}Fe_{0.2}Co_{0.2}Mn_{0.2}Ti_{0.1}Cu_{0.1}O_2$	0.898	0.200	0.199	0.198	0.196	0.097	0.100

Table S11. Stoichiometry of NaNFCMTC-2 compounds determined by ICP-MS.

Theoretical chemical formula	Measured atomic ratio						
	Na	Ni	Fe	Co	Mn	Ti	Cu
$Na_{1.0}Ni_{0.2}Fe_{0.2}Co_{0.2}Mn_{0.2}Ti_{0.1}Cu_{0.1}O_2$	0.996	0.198	0.200	0.196	0.198	0.098	0.101

Table S12. Electrochemical performance of the reported O3 type high-entropy cathodes for sodium-ion batteries.

Cathode	Voltage range	Initial capacity	Capacity retention	Rate performance	Ref
$NaNi_{1/4}Co_{1/4}Fe_{1/4}Mn_{1/8}Ti_{1/8}O_2$	2.0−4.1 V	128 mAh g^{-1}	97.7% after 100 cycles (2 C)	62.3 mAh g^{-1} (30C)	[S5]
$Na_{0.8}Ni_{0.2}Fe_{0.2}Co_{0.2}Mn_{0.2}Ti_{0.2}O_2$	2.0−4.0 V	107 mAh g^{-1}	90% after 100 cycles (0.05 C)	94.1 mAh g^{-1} (5C)	[S6]

$NaNi_{0.12}Cu_{0.12}Mg_{0.12}Fe_{0.15}Co_{0.15}Mn_{0.1}Ti_{0.1}Sn_{0.1}Sb_{0.04}O_2$	2.0−3.9 V	110 mAh g^{-1}	83% after 500 cycles (3.0 C)	87.1 mAh g^{-1} (5C)	[S7]
$NaFe_{0.2}Co_{0.2}Ni_{0.2}Ti_{0.2}Sn_{0.1}Li_{0.1}O_2$	2.0−4.1 V	112.7 mAh g^{-1}	67% after 200 cycles (0.5 C)	80.8 mAh g^{-1} (2C)	[S8]
$Na_{2/3}Li_{1/6}Fe_{1/6}Co_{1/6}Ni_{1/6}Mn_{1/3}O_2$	2.0−4.5 V	171.2 mAh g^{-1}	63.7% after 300 cycles (5 C)	78.2 mAh g^{-1} (10C)	[S9]
$NaCu_{0.1}Ni_{0.3}Fe_{0.2}Mn_{0.2}Ti_{0.2}O_2$	2.0−3.9 V	130 mAh g^{-1}	70.8% after 500 cycles (0.5 C)	85 mAh g^{-1} (5C)	[S10]
$NaNi_{0.25}Mg_{0.05}Cu_{0.1}Fe_{0.2}Mn_{0.2}Ti_{0.1}Sn_{0.1}O_2$	2.0−4.0 V	130.8 mAh g^{-1}	75% after 500 cycles (1 C)	108 mAh g^{-1} (5C)	[S11]
$NaNi_{0.1}Mn_{0.15}Co_{0.2}Cu_{0.1}Fe_{0.1}Li_{0.1}Ti_{0.15}Sn_{0.1}O_2$	2.0−4.1 V	115.0 mAh g^{-1}	82.7% after 1000 cycles (160 mA g^{-1})	≈ 92 mAh g^{-1} (160 mA g^{-1})	[S12]
$Na_{0.89}Li_{0.05}Cu_{0.11}Ni_{0.11}Fe_{0.3}Mn_{0.43}O_{1.97}F_{0.03}$	1.5−4.0 V	146 mAh g^{-1}	80% after 300 cycles (1 C)	109 mAh g^{-1} (10C)	[S13]
$Na_{0.83}Li_{0.1}Ni_{0.25}Co_{0.2}Mn_{0.15}Ti_{0.15}Sn_{0.15}O_{2-\delta}$	2.0−4.2 V	109.4 mAh g^{-1}	87.2% after 200 cycles (2 C)	83.3 mAh g^{-1} (10C)	[S14]
$Na_{0.9}Ni_{0.2}Fe_{0.2}Co_{0.2}Mn_{0.2}Ti_{0.15}Cu_{0.05}O_2$	2.2−4.1 V	117.8 mAh g^{-1}	79.4% after 2000 cycles (5 C)	98.6 mAh g^{-1} (10C)	This work

Table S13. Na^+ diffusion coefficients calculated from CV curves at different scan rates.

Cathode	D_{Na+} of peak a ($cm^2\ s^{-1}$)	D_{Na+} of peak b ($cm^2\ s^{-1}$)
NaNFCMTC-0	4.45×10^{-12}	7.94×10^{-13}
NaNFCMTC-0'	4.33×10^{-12}	9.19×10^{-13}
NaNFCMTC-1	1.26×10^{-11}	7.34×10^{-12}
NaNFCMTC-2'	1.38×10^{-11}	4.28×10^{-12}
NaNFCMTC-2	1.48×10^{-11}	6.83×10^{-12}

Table S14. Impedance results obtained from EIS fitting with the equivalent circuit.

Cathode	R_s/Ω	R_{sf}/Ω	R_{ct}/Ω	R_w/Ω
NaNFCMTC-0	11.0	266.2	451.6	3865.0
NaNFCMTC-0'	8.4	247.7	1749.0	2973.0
NaNFCMTC-1	8.9	157.2	1049.0	1639.0
NaNFCMTC-2'	11.0	692.5	1306.0	2432.0
NaNFCMTC-2	7.8	974.4	2645.0	3116.0

References

[S1] a) G. Kresse, J. Furthmüller, *Phys. Rev. B* **1996**, 54, 11169; b) G. Kresse, J. Furthmüller, *Comp. Mater. Sci.* **1996**, 6, 15.
[S2] J. P. Perdew, K. Burke, M. Ernzerhof, *Phys. Rev. Lett.* **1996**, 77, 3865.

[S3] H. H. Pham, G. T. Barkema, L.-W. Wang, *Phys. Chem. Chem. Phys.* **2015**, 17, 26270.
[S4] a) H.-R. Yao, P.-F. Wang, Y. Wang, X. Yu, Y.-X. Yin, Y.-G. Guo, *Adv. Energy Mater.* **2017**, 7, 1700189; b) Z. Zeng, L. Y. Gan, H. Bin Yang, X. Su, J. Gao, W. Liu, H. Matsumoto, J. Gong, J. Zhang, W. Cai, Z. Zhang, Y. Yan, B. Liu, P. Chen, *Nat. Commun.* **2021**, 12, 4088; c) S. Zhao, Q. Shi, R. Qi, X. Zou, J. Wang, W. Feng, Y. Liu, X. Lu, J. Zhang, X. Yang, Y. Zhao, *Electrochim. Acta* **2023**, 441, 141859.
[S5] J.-L. Yue, W.-W. Yin, M.-H. Cao, S. Zulipiya, Y.-N. Zhou, Z.-W. Fu, *Chem. Commun.* **2015**, 51, 15712.
[S6] D. A. Anang, J.-H. Park, D. S. Bhange, M. K. Cho, W. Y. Yoon, K. Y. Chung, K.-W. Nam, *Ceram. Int.* **2019**, 45, 23164.
[S7] C. Zhao, F. Ding, Y. Lu, L. Chen, Y.-S. Hu, *Angew. Chem. Int. Ed.* **2020**, 59, 264.
[S8] K. Tian, H. He, X. Li, D. Wang, Z. Wang, R. Zheng, H. Sun, Y. Liu, Q. Wang, *J. Mater. Chem. A* **2022**, 10, 14943.
[S9] L. Yao, P. Zou, C. Wang, J. Jiang, L. Ma, S. Tan, K. A. Beyer, F. Xu, E. Hu, H. L. Xin, *Adv. Energy Mater.* **2022**, 12, 2201989.
[S10] C.-C. Lin, H.-Y. Liu, J.-W. Kang, C.-C. Yang, C.-H. Li, H.-Y. T. Chen, S.-C. Huang, C.-S. Ni, Y.-C. Chuang, B.-H. Chen, C.-K. Chang, H.-Y. Chen, *Energy Storage Mater.* **2022**, 51, 159.
[S11] F. Ding, C. Zhao, D. Xiao, X. Rong, H. Wang, Y. Li, Y. Yang, Y. Lu, Y.-S. Hu, *J. Am. Chem. Soc.* **2022**, 144, 8286.
[S12] X.-Y. Du, Y. Meng, H. Yuan, D. Xiao, *Energy Storage Mater.* **2023**, 56, 132.
[S13] F. Ding, H. Wang, Q. Zhang, L. Zheng, H. Guo, P. Yu, N. Zhang, Q. Guo, F. Xie, R. Dang, X. Rong, Y. Lu, R. Xiao, L. Chen, Y.-S. Hu, *J. Am. Chem. Soc.* **2023**, 145, 13592.
[S14] H. Wang, X. Gao, S. Zhang, Y. Mei, L. Ni, J. Gao, H. Liu, N. Hong, B. Zhang, F. Zhu, W. Deng, G. Zou, H. Hou, X.-Y. Cao, H. Chen, X. Ji, *ACS Nano* **2023**, 17, 12530.